

Cellular automata dynamics of nonlinear optical processes in a phase-change material



Cite as: Appl. Phys. Rev. **8**, 011404 (2021); <https://doi.org/10.1063/5.0015363>

Submitted: 27 May 2020 . Accepted: 21 December 2020 . Published Online: 03 February 2021

Liwei Zhang, Robin F. Waters, Kevin F. MacDonald, and Nikolay I. Zheludev

COLLECTIONS



This paper was selected as Featured



View Online



Export Citation



CrossMark

Applied Physics Reviews

Impact matters.

17.054

JOURNAL IMPACT FACTOR

Cellular automata dynamics of nonlinear optical processes in a phase-change material

Cite as: Appl. Phys. Rev. **8**, 011404 (2021); doi: [10.1063/5.0015363](https://doi.org/10.1063/5.0015363)

Submitted: 27 May 2020 · Accepted: 21 December 2020 ·

Published Online: 3 February 2021



View Online



Export Citation



CrossMark

Liwei Zhang,^{1,2}  Robin F. Waters,¹ Kevin F. MacDonald,^{1,a)}  and Nikolay I. Zheludev^{1,3} 

AFFILIATIONS

¹Optoelectronics Research Centre & Centre for Photonic Metamaterials, University of Southampton, Highfield, Southampton SO17 1BJ, United Kingdom

²School of Mathematics and Physics, Anqing Normal University, Anqing 246133, People's Republic of China

³Centre for Disruptive Photonic Technologies & The Photonics Institute, School of Physical and Mathematical Sciences, Nanyang Technological University, Singapore 637371

^{a)}Author to whom correspondence should be addressed: kfm1@soton.ac.uk

ABSTRACT

Changes in the arrangement of atoms in matter, known as structural phase transitions or phase changes, offer a remarkable range of opportunities in photonics. They are exploited in optical data storage and laser-based manufacturing, and have been explored as underpinning mechanisms for controlling laser dynamics, optical and plasmonic modulation, and low-energy switching in single nanoparticle devices and metamaterials. Comprehensive modeling of phase-change processes in photonics is, however, extremely challenging as it involves a number of entangled processes including atomic/molecular structural change, domain and crystallization dynamics, change of optical properties in inhomogeneous composite media, and the transport and dissipation of heat and light, which happen on time and length scales spanning several orders of magnitude. Here, for the first time, we show that the description of such complex nonlinear optical processes in phase-change materials can be reduced to a cellular automata model. Using the important example of a polymorphic gallium film, we show that a cellular model based on only a few independent and physically-interpretable parameters can reproduce the experimentally measured behaviors of gallium all-optical switches over a wide range of optical excitation regimes. The cellular automata methodology has considerable heuristic value for the study of complex nonlinear optical processes without the need to understand details of atomic dynamics, band structure, and energy conservation at the nanoscale.

Published under license by AIP Publishing. <https://doi.org/10.1063/5.0015363>

I. INTRODUCTION

Sixty years after the invention of the laser, light-induced structural phase transitions continue to fascinate the photonics research community: The study of optical properties provides insight to the fundamental physics of material properties, transition mechanisms and dynamics, and they have had a transformational impact on society, for example, in the guise of optical data storage technologies^{1,2} (CDs and DVDs) and as the underpinning of laser-based manufacturing processes, from cutting and welding metals, dielectrics, and semiconductors, to laser-based additive and direct-write micro/nanofabrication techniques.^{3–8} In photonics, materials undergoing light-induced phase transitions, in particular between states with markedly different optical properties, provide a rich variety of functionalities for controlling light-with-light.^{9–12}

- Chalcogenide semiconductor “glasses” undergoing optically-induced, nonvolatile amorphous-crystalline state transitions have

long been the foundation of rewritable data storage. Lately, among numerous emerging applications of chalcogenides in photonics,^{13–15} as optically-addressed phase-change media they have facilitated the realization of optically switchable plasmonic metamaterials and nano-antennas, waveguide modulators, and all-dielectric metasurfaces, providing high-contrast free-space and guided-wave signal modulation relevant to a variety of communications, imaging and sensing applications, rewritable and active flat optical elements that can dramatically reduce the size and weight of optical systems and are one of the key material platforms in the burgeoning fields of optical RAM (random access memory) and photonic neuromorphic computing.^{16,17}

Sámson *et al.* first demonstrated the principle of plasmonic modulation through reversible photo-induced changes in a chalcogenide¹⁸-modulating the Kretschmann geometry coupling of near-infrared light to surface plasmon polaritons at a

silver/ chalcogenide (gallium lanthanum sulphide, GLS) interface via low intensity white light-induced photo-darkening/refraction.

Gholipour *et al.* presented the first metamaterial all-optic switch with functionality underpinned by chalcogenide phase change—a planar plasmonic metasurface hybridized with a thin film of germanium antimony telluride ($\text{Ge}_2\text{Sb}_2\text{Te}_5$ or GST-225),¹⁹ in which reversible, nonvolatile amorphous-crystalline transitions provide near- and mid-infrared transmission and reflection modulation contrast ratios of 4:1 in devices of substantially sub-wavelength thickness (down to 1/27 of the operating wavelength), with active domains as large as $2000\ \mu\text{m}^2$ switched by single nanosecond laser pulses. Karvounis *et al.* subsequently demonstrated a nanostructured all-chalcogenide (GST-225) dielectric metasurface in which spectral shifting of resonances brought about through laser-induced crystallization delivers reflectivity and transmission switching contrast ratios of up to 5:1 at visible/near-infrared wavelengths selected by design.²⁰

Rudé *et al.* have utilized GST-225 to control the propagation of near-infrared surface plasmon-polaritons (SPPs) on a Au-SiO₂ interface²¹ and of light in silicon photonic waveguides,²² in both cases, crystallization of a thin amorphous GST cladding layer induced by sub-microsecond laser pulses increases the GST refractive index and absorption coefficient, thereby inhibiting plasmonic/photonic signal propagation in the waveguides.

Michel *et al.* have demonstrated reversible, nonvolatile switching of infrared plasmonic (aluminum) antenna array resonances via femtosecond-pulse laser-induced switching of a 50-nm GST-326 coating²³ and “programmable” phase switching of the coating around individual metamolecules within an array of nanorod resonators using single sub-microsecond laser pulses.²⁴

Femtosecond (fs) pulses have also been employed by Wang *et al.* for “grayscale” phase switching of GST-225: tailored trains of fs pulses are used to achieve discrete reproducible levels of partial crystallization in diffraction-limited domains of a thin GST film, enabling Gbit/in² (non-binary) optical data storage²⁵ and the realization of laser-rewritable flat lenses and holographic optical elements.²⁶ Active flat optical components have also been realized; for example, Ruiz de Galarreta *et al.* have demonstrated a beam-steering device with no moving parts based on a phase-gradient metasurface hybridized with a thin film of GST, switched by near-ultraviolet/visible (405 nm) laser irradiation.²⁷

The incremental grayscale “accumulation” property of chalcogenide phase-change media is essential to their application in photonic neuromorphic (brain-inspired) computing, wherein, for example, phase-change cells patterned onto photonic waveguides provide optical neuron and synapse functionalities.²⁸

- Similarly, the volatile semiconductor-metal transition in vanadium dioxide (VO_2 ; occurring at $\sim 68^\circ\text{C}$) has been and continues to be investigated for a wide variety of optically-addressed active plasmonic and photonic applications at visible, infrared, THz, and microwave frequencies.²⁹

The ultrafast dynamics of VO_2 's solid–solid phase transition were first interrogated optically by Becker *et al.*³⁰ and later by Cavalleri *et al.* using a fs optical pump/x-ray probe technique,³¹ with results suggesting that in this regime the transition is initiated non-thermally. More recent works have suggested that the ultrafast transition in VO_2 involves a transient excited electronic (metallic) state retaining the monoclinic (ground state) structure.^{32–36}

Rini *et al.* subsequently studied the ultrafast optical response of VO_2 nanoparticles,³⁷ observing a large, light-induced ultrafast enhancement of optical absorption in the near-infrared spectral range. Optical-pump, THz-probe techniques have followed.^{38,39}

Muskens *et al.* have also recently reported on antenna (localized surface plasmon resonance)-assisted picosecond control of nanoscale phase transitions in VO_2 , with switching energies 20 times lower and recovery times 5 times faster than in bare VO_2 films.⁴⁰

Many of the architectures developed for VO_2 -plasmonic hybrid and all- VO_2 metamaterials/surfaces with switchable resonant reflection/transmission characteristics, and guided-wave switching devices, mirror those of their chalcogenide-based counterparts (above).^{41–45}

However, as a consequence of the volatile nature of the metal-semiconductor transition in VO_2 , these almost invariably rely on ambient temperature change rather than optical excitation to induce transitions. Recent exceptions to this rule include, for example, the demonstration by Lei *et al.* of a nanoscale memory effect in gold nanodisk arrays on VO_2 excited by ultraviolet optical pulses, wherein plasmon resonance modulation depends strongly on the initial state,⁴⁶ and the demonstration of a limiting “optical diode” based on the asymmetrically nonlinear transmission characteristic of a nanoscale gold/ VO_2 bilayer.⁴⁷

- Elemental gallium (Ga) subject to nanoscale, optically-driven “surface melting” in proximity to the near-ambient bulk melting point (29.8°C) or solid–solid transitions among crystalline forms in confined (e.g., nanoparticle) geometries at cryogenic temperatures is the medium for which the terms “phase-change non-linearity” and “active plasmonic” were coined.

Its ability to provide a gigantic, broadband optical nonlinearity via light-induced structural change (between solid and liquid states with markedly different optical properties, as opposed to the conventional purely electronic mechanism of nonlinear optical response) was first reported by Bennet *et al.*: a Ga mirror formed at the tip of a single-mode optical fiber being shown to provide for cross-wavelength light-by-light modulation in the telecommunications C-band at milliwatt power levels.⁴⁸

Petropoulos *et al.* subsequently harnessed this nonlinearity for passive Q-switching of erbium and ytterbium fiber lasers,⁴⁹ achieving a level of performance (a self-starting regime generating ~ 50 -ns pulses with peak powers up to 100 W) equivalent to that of state-of-the-art, narrowband semiconductor saturable absorbers.

Recently, Waters *et al.* have shown that gallium's phase-change nonlinearity can be resonantly enhanced by an order of magnitude in a photonic metamaterial architecture,⁵⁰ to offer high-contrast, all-optical, near-infrared switching at $\mu\text{W}/\mu\text{m}^2$ excitation intensities.

Gallium's phase-change nonlinearity was the basis of the original “active plasmonics” concept,⁵¹ whereby propagation of SPPs on a metal–dielectric waveguide interface can be modulated with high contrast via induced changes in the optical properties of one of the two materials, occurring only within a few nanometers of the surface. Krasavin *et al.* demonstrated optical modulation of SPP coupling at a Ga–dielectric interface using few-ns near-infrared pulses to drive transient nanoscale melting of the metal, both in its bulk form and as a composite with aluminum (formed by grain boundary penetration of liquid Ga into an Al thin film),^{52,53} Vivekchand *et al.* demonstrated thermally-tuned control of SPP coupling using Ga grating.⁵⁴

In monolayer ensembles of Ga nanoparticles (fabricated via optically-controlled self-assembly) a phase-change optical nonlinearity associated with light-induced melting of the ‘metastable’ β , γ and/or δ solid phases (which are preferentially formed over the α -phase in highly-confined geometries) was first reported by MacDonald *et al.*^{55–57} Soares *et al.* subsequently demonstrated single-nanoparticle optical gating and optical memory functionalities based upon optical switching among the several different structural forms at few-pJ optical pulse switching energies.^{58–61} Pochon and Denisjuk *et al.* further explored combinations of optical and electron beam controlled phase-coexistence with optical and cathodoluminescent ‘read-out’ of Ga phase state in nanoparticle memories.^{62,63} The unusual polymorphism of gallium is now drawing renewed attention in the context of UV plasmonics.^{64,65}

Depending on incident fluence and photon energy, target size/shape/structure, and ambient conditions, optically-induced transitions in any material may proceed through a combination of thermal and/or non-thermal mechanisms on electronic/atomic to macroscopic length scales at femto- to millisecond timescales. Optical measurements, which are based predominantly on interactions between photons and valence or delocalized electrons, cannot directly resolve atomic-scale mechanisms of structural transition. *Ab initio* computational methods, like density functional theory, molecular dynamics, kinetic equations, or combinations thereof, can provide insight to behaviors and mechanisms at the atomic level^{66,67} but are computationally demanding and typically cannot span the full range of length and/or timescales involved. Similar constraints apply to numerical, finite element and finite difference time domain, multiphysics simulations. Alternative approaches to describing phase transition processes, capable of encompassing disparate length/timescales, are offered by rate equations,^{68,69} phase field methods,^{70,71} Monte Carlo models,⁷² and, as considered here, cellular automata (CA).^{73–78} Indeed, CA have been applied to modeling dynamics in a remarkable diversity of complex systems, from laser emission to the growth of snowflakes and from ionic diffusion in concrete to pattern recognition in networks,^{79–82} as well as the melting and solidification (crystal nucleation/growth/dissociation) of materials.^{73–78} However, when considering nominally laser-driven structural transitions, these models tend simply to assume the existence of a heat source, i.e., disregard non-thermal excitation and feedback between the induced change in material properties and the rate of energy deposition. CA models are rarely encountered in the field of optics and photonics because the propagation of light and many of its interactions with matter are very well described either analytically or, for example in complex nanostructured media, via finite element and finite difference time domain “Maxwell solver” numerical simulation techniques. Some exceptions to this rule are found in the domain of quantum/optical computing (especially quantum dot cellular automata^{83–88}), occasionally in the study of photonic dynamics (e.g., laser level populations,⁷⁹ frequency comb spectral perturbations,⁸⁹ collective behaviors in VCSEL arrays⁹⁰) and in adaptation of the classic “Game of Life” evolutionary CA model to account for the retrieval of energy from an environment filled by an electromagnetic field⁹¹ (leading to behaviors such as light-induced self-structuring and genetic selection). While the numerical methods mentioned above can encompass “multiphysics” (e.g., light-induced heating), they rapidly become opaque in their complexity and

computationally prohibitive where disparate length and timescales are involved and where dynamic structural changes have a strong and nonlinear effect on optical properties. Here, we apply a CA methodology for the first time to photo-induced structural transitions in and the associated instantaneous nonlinear optical response of a metal, specifically gallium, as a medium in which a strong non-thermal component of response is known to manifest under certain regimes of excitation. The approach offers high heuristic value in its simplicity, with the model being defined by a small set of material parameters and others relatable to experimental observables, and practicality, being adaptable to a wide variety of material systems and nano- to macroscopic geometries.

Gallium is an unusually polymorphic element, with several structural phases that have properties ranging from those of the liquid, which is a highly reflective, near-ideal free-electron metal at optical frequencies,^{92,93} to those of the stable bulk crystalline form, known as α -gallium, which is considerably less “metallic” in character (less reflective, more absorbing).^{94,95} α -Gallium has a structure in which molecular and metallic properties coexist: some inter-atomic bonds are covalent, forming Ga_2 dimers and giving rise to a broad optical absorption band extending from 310 to 1820 nm, while the rest are metallic.^{94,96} It also manifests “surface melting,”⁹⁷ whereby a thin (few nm) layer of metallic gallium is formed between the solid α -phase and a dielectric even at temperatures several degrees below T_m . The thickness of this interfacial layer, and thereby the reflectivity of the interface, can be controlled in a continuously tunable fashion by low-intensity laser illumination. These characteristics together make gallium a uniquely intriguing and richly functional photonic material, but also one in which it is difficult to interpret or disentangle underlying response mechanisms. The dynamics of light-induced reflectivity changes at gallium–dielectric interfaces, and their dependence on intensity or fluence and the temperature of the bulk metal, have been studied under various regimes of pulsed optical excitation.^{98–100} At the shortest (fs to ps) timescales, non-equilibrium electronic excitation dominates the reflective response; at longer timescales, thermal effects (i.e., laser-induced heating) alone are insufficient to account for observed dependences of induced reflectivity change on temperature, and a substantive non-thermal contribution to interfacial metallization (based on the direct optical excitation of the dimer covalent bonds in α -gallium) is inferred. We find here that reflectivity dynamics at a gallium–dielectric interface are elegantly described for the full range of fs to μs pulse durations by a simple three-level CA model including a non-thermal excitation channel, operating under a minimal set of transition rules that are invariant with pulse duration.

Cellular automata are fully discrete dynamic systems, wherein the state of each cell in a regular n -dimensional lattice is chosen from a finite set of possible states and temporal evolution runs synchronously in all cells.^{101,102} Each cell evolves in each time step according to a set of transition rules dependent on its initial state and those of other cells within a defined (e.g., von Neumann, Moore) neighborhood. Here, we have constructed a two-dimensional CA model of minimally sufficient complexity (see Sec. IV, METHODS) to describe the photo-induced metallization dynamics of Ga at a planar gallium–silica interface. Each gallium cell [Fig. 1(a)] can exist in one of three states [Fig. 1(b)]: a lowest-energy “ground” state (level 1), a higher-energy “metallic” state (level 2), and a highest-energy, short-lived “optically excited” state (level 3). The ground state possesses optical properties identical to

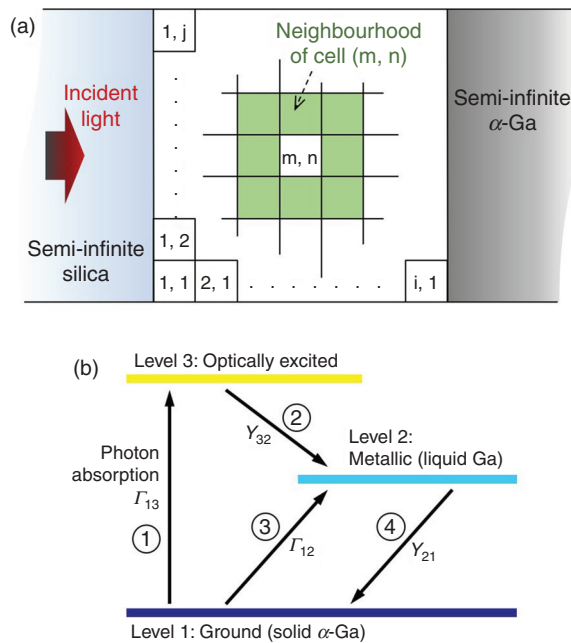


FIG. 1. Cellular automata model of a gallium–silica interface. (a) Schematic of the 2D cellular array and the adjacent semi-infinite silica and solid gallium volumes assumed to be present in the evaluation of interface reflectivity. Each Ga cell can exist in one of three states as shown in panel (b): a lowest-energy “ground” state; a higher-energy metallic state; and a highest-energy, short-lived “optically excited” state. (b) Three-level system of gallium cell states and associated transitions, annotated with transition probabilities (Γ , γ) and accompanying CA transition rule numbers (circled).

those of α -gallium,⁹⁵ while the optically excited state and metallic states possess the optical properties of liquid gallium.⁹² Γ_{13} is the optical pumping rate driving excitation from the ground state (1) to the excited state (3) and depends on the incident photon flux, i.e., incident light intensity, which in turn is a function of time t , i.e., pulse duration and profile. Γ_{12} is the rate of thermally-induced transition from the ground state (1) to the metallic state (2) and depends on the proximity of local temperature to T_m . As such, it is a function of both ambient temperature (tending exponentially to one as $T \rightarrow T_m$ and to zero as $[T_m - T]$ increases) and light-induced temperature change (i.e., pulse duration, profile, and fluence). γ_{32} and γ_{21} are, respectively, the decay probabilities from the excited state (3) to metallic state (2) and from the metallic state (2) to the ground state (1) within a single time step δt (see [supplementary material](#), Fig. S1).

The evolution of each cell in each time step is governed by a set of four rules:

- **Rule 1.** Cells in the GROUND state become EXCITED if they absorb a photon (the probability of absorption being a function of the optical skin depth; see [supplementary material](#)).
- **Rule 2.** Cells in the EXCITED state decay to the METALLIC state with a probability γ_{32} , given by the lifetime of the excited state τ_3 : $\gamma_{32} = 1 - e^{-\delta t/\tau_3}$.
- **Rule 3.** Cells in the GROUND state are converted to the METALLIC state: (1) with a probability Γ_{12} when the number of neighboring cells (among the eight surrounding, i.e., nearest and

next-nearest) already in the METALLIC or EXCITED state is greater than 1 and less than or equal to a threshold N_{12} , and (2) with certainty (probability = 1) when the number of METALLIC or EXCITED neighbors is greater than N_{12} .

- **Rule 4.** Cells in the METALLIC state decay to the GROUND state with a probability $\gamma_{21} = 1 - e^{-\delta t/\tau_2}$, where τ_2 is the lifetime of the metallic state, when the number of METALLIC or EXCITED neighbors is less than or equal to a threshold N_{21} .

Rules 1 and 2 describe the non-thermal photo-induced metallization process, whereby the absorption of a photon leads to the breaking of a Ga–Ga dimer bond and the structural reconfiguration of the associated unit cell in the atomic lattice. Rules 3 and 4 describe the balance between metallization (cf. melting) and recrystallization of cells based effectively on the transfer of absorbed energy from electrons to the lattice and from cell-to-cell through the lattice, and/or on changes in the energetically-preferred configuration of ground-state cells surrounded by numerous metallic cells, and vice versa. (Schematic dependences of transition probabilities on neighborhood are shown in [supplementary material](#), Fig. S2.)

The lifetimes of the excited and metallic states are set, respectively, at $\tau_3 = 1$ ps and $\tau_2 = 1$ ns. Exact values for gallium are not known, so these are representative, order-of-magnitude values¹⁰³ sufficient for the present purpose of a self-consistent comparison among metallization dynamics across a range of pulsed optical excitation regimes. Indeed, we specifically do not aspire to quantitatively replicate any particular set of prior experimental data, and as results will illustrate (see Sec. II), it is relative rather than absolute values of lifetimes and pulse duration that determine behaviors within the CA model. A third time constant of importance is the “thermalization time” τ_t , over which heat is dissipated from the region in which it is generated through photon absorption. This nonlinear heat flow (dependent on both spatial and temporal pulse profile, sample structure, and ambient temperature) can lead to complex reflectivity relaxation dynamics.^{98,99} For the CA model, we again assume a representative, suitably physical, order-of-magnitude value $\tau_t = 1$ μ s.

II. RESULTS AND DISCUSSION

We first consider the short-pulse excitation regime, with a CA model time step δt of 1 fs and (pump) pulse duration τ_p of 100 steps, i.e., 100 fs, centered at time step 150. [Figure 2\(a\)](#) shows the dynamics of interface reflectivity at the $\lambda = 775$ nm pump wavelength (cf. frequency degenerate pump-probe measurements) for a range of excitation fluences, with neighbor threshold values N_{21} , $N_{12} = 5$ and a transition probability $\Gamma_{12} = 8 \times 10^{-5}$ (see [supplementary material](#)). In general, Γ_{12} is a function of incident fluence (and therefore time during a Gaussian excitation pulse) and temperature, but in the femtosecond regime, it can be taken as constant during and considerably beyond the pulse duration because δt , $\tau_p \ll \tau_2$, τ_t . Reflectivity dynamics are correspondingly dominated by the photo-excitation channel. For the same reason, the values of N_{12} and N_{21} are found to be of negligible consequence to response dynamics within the first several picoseconds during and after a fs pulse (see [supplementary material](#), Fig. S4), which is to say that on such timescales, the state of each cell evolves independently, without influence from its neighbors.

Reflectivity dynamics are characterized, as in corresponding experimental studies,^{99,100} by a sharp increase in reflectivity during the excitation pulse, to a level that increases with fluence, followed by a

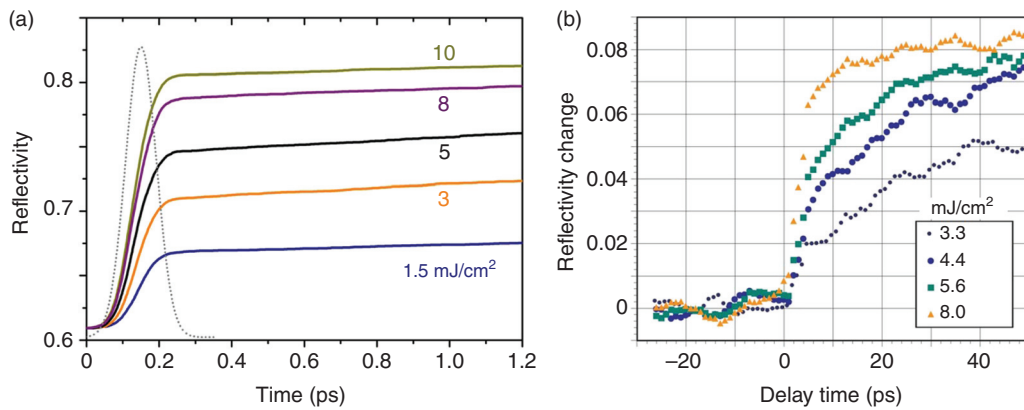


FIG. 2. Reflectivity dynamics in the short-pulse excitation regime. (a) CA modeled Ga-silica interface reflectivity at 775 nm as a function of time [time step $\delta t = 1$ fs] during and immediately after 100-fs pump pulses of varying fluence (as labeled; $N_{12}, N_{21} = 5$; $\Gamma_{12} = 8 \times 10^{-5}$). The dashed gray line shows the Gaussian temporal profile of the excitation pulse (normalized amplitude—vertical axis scale does not apply). (b) Experimentally measured Ga-silica interface reflectivity at 800 nm as a function of time around 150-fs pump pulses of varying fluence (as labeled). Reprinted with permission from A. V. Rode *et al.*, *Opt. Lett.* **26**, 441 (2001). Copyright 2001 The Optical Society.⁹⁹ Note that the full 1.2-ps span of panel (a) corresponds to a small fraction of the axial range in panel (b).

much longer and shallower rise over picosecond timescales after the pulse, as shown in Fig. 2(b). Snapshots of phase state distribution at representative time intervals are presented in Figs. 3(a)–3(h) (a full video file of phase state evolution with single time step resolution is available online) and show that this is a consequence of a rapid (non-thermal) increase in the population of cells in the EXCITED state during the pulse. These are randomly distributed with a number density that decreases exponentially, as one would expect, with distance from the gallium–glass interface. These transition to the METALLIC state and thermal (neighbor interaction) mechanisms then dominate on picosecond timescales and beyond, sustaining an upward trend in reflectivity (based on rule 3) for some time after the pulse. Note here that at all points in the gallium bulk (beyond the persistent surface-melt layer at the glass interface), melting is “incomplete” even at long time intervals after the excitation pulse; there is no continuously molten layer of defined fluence-, temperature-, and time-dependent depth. The structure of METALLIC inclusions in a GROUND state matrix (or vice versa close to the interface) seen in the CA model is consistent with prior analytical inference of fractional light-induced melting from reflectivity measurements in the fs-pulsed excitation regime.¹⁰⁰

We now consider the very substantial effect of pulse duration on metallization dynamics. In the CA model, this is achieved by maintaining a fixed pulse duration τ_p of 100 time steps (centered at step 150) while changing the step size δt , in the present case from 1 fs to 10 ns in seven order-of-magnitude increments. We maintain near-neighbor threshold values $N_{12}, N_{21} = 5$ and assume a fixed fluence of $F_{in} = 5$ mJ/cm² across all pulse durations.

Figures 4(a)–4(h) show snapshot phase-state distributions at the 150th time step, i.e., at the peak of the pulse when photon flux is at maximum, for pulse durations ranging from 100 fs to 1 μ s. (A corresponding set of snapshots for the 250th time step, in the tail of the pulse, is shown in supplementary material, Fig. S5). For short pulse durations ≤ 1 ns [Figs. 4(a)–4(e)], i.e., shorter than the metallic state lifetime τ_2 , there is a diffuse population of cells in the optically excited and/or metallic state. This extends, with decaying number density, over several skin depths into the gallium bulk with almost no change

in the thickness of the persistent surface-melt layer at the glass interface. There is a significant proportion of excited-state cells only for pulse durations ≤ 10 ps [Figs. 4(a)–4(c)], i.e., while the time step δt remains shorter than the excited state lifetime τ_3 (for durations > 10 ps but ≤ 1 ns, cells excited in a given time step will transition to the metallic state with near-certainty in the next).

This diffuse, non-equilibrium (non-thermal) distribution of excited/metallic cells is responsible for the two-stage, fast and then much slower, interface reflectivity dynamic that is characteristic of short-pulse excitation regimes [as illustrated in supplementary material, Figs. S6(a)–S6(e)]. It is entirely absent for pulse durations ≥ 100 ns [Figs. 4(g) and 4(h)] because any isolated metallic cells revert to the ground state with near certainty ($\gamma_{21} \rightarrow 1$) in every time step. Cells can only be sustained in the metallic state for more than one time step by the neighbor rules, which is to say thermally. This leads to contiguous “growth” of the surface-melt layer into the gallium bulk and a proportionate, steady increase in interface reflectivity over the duration of the pulse [supplementary material, Figs. S6(g) and S6(h)].

Figure 4(f), for a pulse duration of 10 ns, shows characteristics of both the short- and longer-pulse regimes, i.e., both a not-insignificant population of individual/clustered metallic-state cells within the ground-state bulk and a clear change in the thickness of the interfacial surface-melt layer. Reflectivity dynamics [supplementary material, Fig. S6(f)] are correspondingly mixed, showing elements of both a fast initial increase and a slower, steady change over the pulse duration. This intermediate case illustrates how the boundary between thermal and non-thermal melting regimes is predominantly a function of metallic state lifetime τ_2 (assuming that τ_3 will always be $\ll \tau_2$).

In the long-pulse (≥ 100 ns) regime, once state lifetimes (τ_2, τ_3) and neighbor thresholds (N_{12}, N_{21}) are set, reflectivity dynamics for a given fluence become a function solely of Γ_{12} , the local-temperature-dependent probability of transition from the ground to the metallic state. For square optical pulses shorter than the thermalization time ($\tau_p < \tau_t$) incident on a sample at a fixed ambient (bulk gallium) temperature, Γ_{12} can be taken as constant over the pulse with a value effectively proportional to the magnitude of light-induced temperature

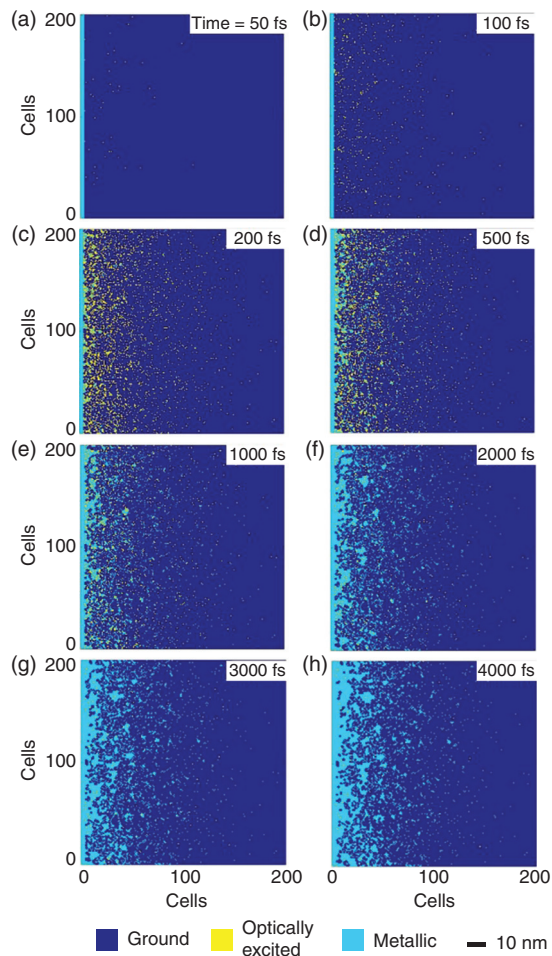


FIG. 3. Temporal evolution of phase-state distribution among cells in the short-pulse excitation regime. Representative maps of cellular phase state (ground, optically excited, or metallic) at intervals of between 50 and 4000 time steps (as labeled, step $\delta t = 1$ fs) around a 100-fs pump Gaussian pulse of fluence $F_m = 5$ mJ/cm² ($N_{12}, N_{21} = 5$; $\Gamma_{12} = 8 \times 10^{-5}$). The silica interface is at the left-hand side of each panel, and light is incident from that direction. Multimedia view: <https://doi.org/10.1063/5.0015363.1>.

change. In this way, by varying Γ_{12} , with a fixed time step δt of 1 ns, near-neighbor thresholds N_{12}, N_{21} again equal to 5, the CA model is able (Fig. 5) to qualitatively reproduce the experimental results of Ref. 98. In the experiment, the local temperature is a function of incident fluence, but in the CA model, the two are decoupled: photon flux alone—the value of F_{in} —does not affect the effective temperature, which is encapsulated in Γ_{12} . Thus, for the purposes of this analysis, we maintain a fixed value of F_{in} and only change Γ_{12} . Reflectivity (cf. metalized layer thickness) increases monotonously with time over the pulse duration at a rate that increases with the value of Γ_{12} , i.e., with induced local temperature change (in the experiment, with peak incident power). The dependence of reflectivity on time is (near-)linear at lower values of Γ_{12} but saturates at higher values as the metalized layer thickness tends toward the optical skin depth. (The latter behavior is not seen in the experimental case simply for lack of laser power.)

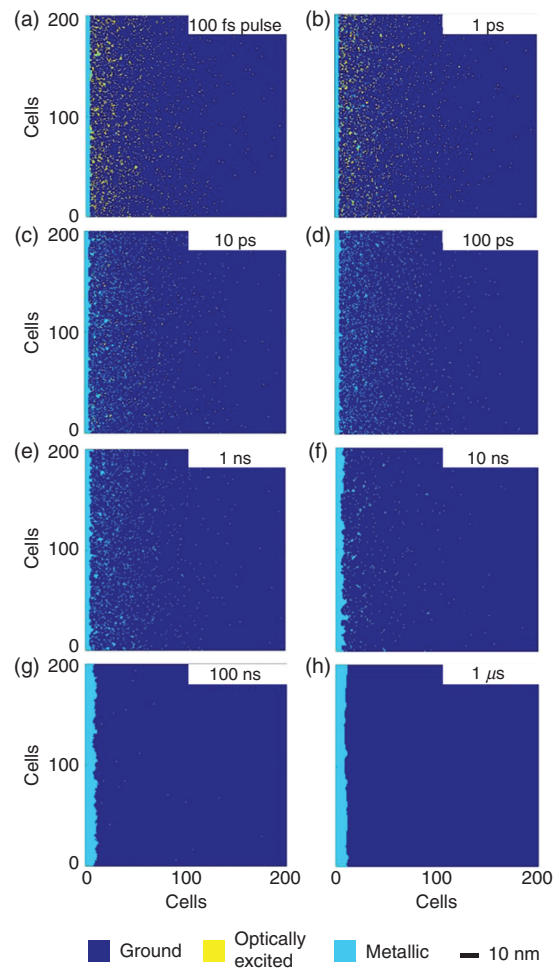


FIG. 4. Phase-state distribution as a function of pulse duration. Representative maps of cellular phase state at the peak of Gaussian excitation pulses with duration τ_p ranging from 100 fs to 1 μ s (as labeled) in order-of-magnitude increments ($F_m = 5$ mJ/cm²; $N_{12}, N_{21} = 5$; $\Gamma_{12} = 8 \times 10^{-5}, 1.2 \times 10^{-4}, 1.5 \times 10^{-4}, 5.2 \times 10^{-4}, 5.25 \times 10^{-3}, 5.65 \times 10^{-2}, 0.465$, and 0.9, respectively).

In contrast to the fs-pulse regime, where they are of negligible consequence, the neighbor thresholds do influence reflectivity dynamics in the long-pulse thermal regime (as shown in [supplementary material](#), Fig. S7)—the effect of changing N_{12} is minor, but the value of N_{21} has a more significant impact. These thresholds are effectively a coarse surrogate for ambient temperature, with lower values corresponding to bulk Ga temperatures closer to T_m , whereby a given fluence can induce a larger change in reflectivity.

When optical excitation is withdrawn, metallic-state cells relax to the α -Ga ground state (i.e., recrystallize) and interface reflectivity correspondingly recovers to its pre-excitation level. This process is governed by the complex, nonlinear dynamics of heat flow and in practice will be a function of pulse duration and spatial and temporal intensity profile, sample structure, and the proximity of ambient (silica and Ga bulk) temperature to T_m . For the purposes of the CA model, characteristic experimentally observed reflectivity relaxation behaviors can be

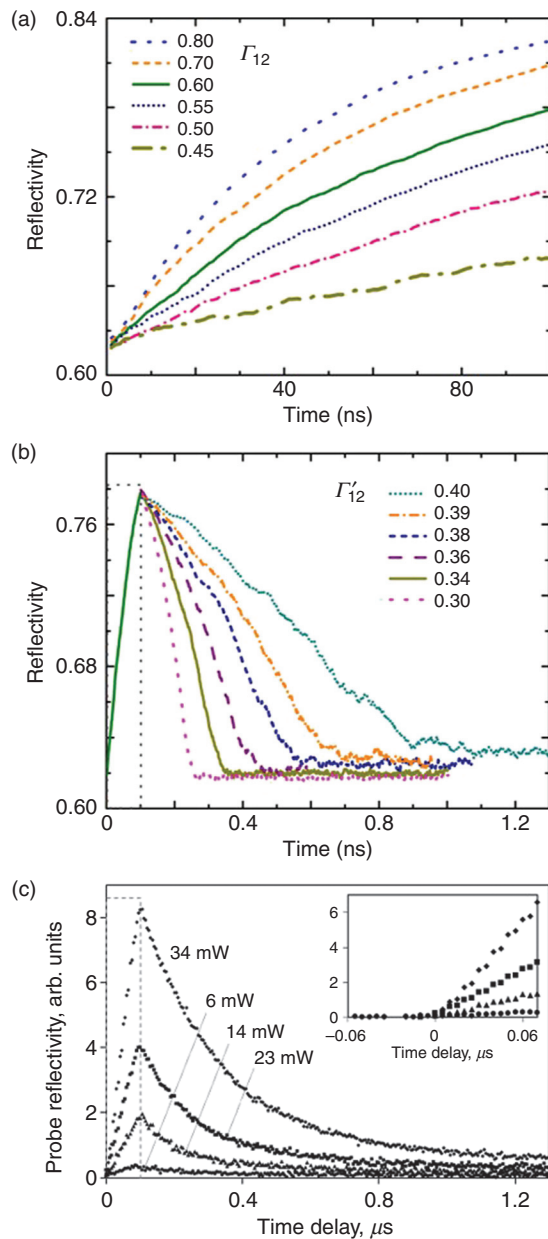


FIG. 5. Reflectivity dynamics in the long-pulse excitation regime. (a) CA modeled Ga-silica interface reflectivity at 775 nm as a function of time (time step $\delta t = 1$ ns) during 100-ns pump pulses, Γ_{12} increase from 0.45 to 0.8. ($F_{in} = 5$ mJ/cm²; $N_{12}, N_{21} = 5$). (b) Interface reflectivity as a function of time after a 100-ns pump pulse ($\Gamma_{12} = 0.6$; $N_{12}, N_{21} = 5$) for a selection of post-excitation transition probabilities Γ'_{12} (as labeled). The dashed black line shows the square temporal profile of the excitation pulse (normalized amplitude—vertical axis scale does not apply). (c) Experimentally measured Ga-silica interface reflectivity at 1550 nm as a function of time during and after excitation with 100-ns 1536-nm pump pulses of varying peak power (as labeled) at a fixed ambient temperature of 24 °C ($T_m - T \sim 5$ °C). The inset shows dynamics near the rising edge of the pump pulse on an expanded timescale. Reprinted with permission from V. Albanis *et al.*, Phys. Rev. B **63**, 165207 (2001). Copyright 2001 American Physical Society.⁹³

qualitatively reproduced [Fig. 5(b)] by simply stepping down the value of Γ_{12} at the end of an excitation pulse. Recall here that this transition rate is essentially a function of local temperature: As such, lower post-excitation values Γ'_{12} can be taken to denote lower ambient temperatures (i.e., higher values of $T_m - T$). Under the course approximation of a step-function in $\Gamma_{12}^{(t)}$ and with the same value of transition probability applying to all cells in the array, the CA model does not replicate the exponential form of the decay curves seen in the experiment [Fig. 5(c)]. However, it is nonetheless sufficient to illustrate that for a given set of excitation conditions, lower ambient temperatures promote faster recrystallization and reflectivity relaxation.

III. SUMMARY

In summary, we show here that a CA model—a three-level system governed by only four transition rules and a sparse set of independent material and process parameters—can phenomenologically describe the complex, non-stationary, spatially inhomogeneous dynamics and resulting nonlinear optical properties of a medium undergoing a light-induced structural phase transition.

We consider the case of solid gallium near its bulk melting transition as a non-trivial system (in which optical excitation may include a strong non-thermal component and surfaces are subject to nanoscale “pre-melting”) of relevance to a variety of photonic (all-optical and “active plasmonic”) switching applications. Non-equilibrium behaviors in systems close to a transition point cannot be described analytically, and they present considerable challenges in computational (e.g., multi-physics finite element) simulation, particularly with regard to the combination of macro- and nanoscopic length scales. In this context, it is remarkable that a CA model (which notably does not include local or ambient temperature as an independently defined parameter) is able to reproduce light-induced transition and relaxation dynamics over seven orders of excitation pulse duration magnitude (from femto- to microsecond) and provide insight to the microscopic mechanisms of transition without recourse to deep understanding or analytical description of atomic dynamics, band structure, electromagnetics, thermodynamics, or nanoscale energy conservation. It emerges clearly from the CA model that transition and reflectivity dynamics in the Ga system are controlled predominantly by the relative values of optically-excited and metallic state lifetimes. These determine whether thermal or non-thermal mechanisms dominate and thereby whether the metallization of α -Ga is diffuse (in the short, fs-ps pulse regime) or proceeds through the motion of a defined solid-liquid melt front (longer pulses). Particularly interestingly, the CA model also shows that neighborhood is essentially irrelevant in the short-pulse excitation regime: at fs timescales there is no coupling between Ga (crystalline) cells, and each cell responds independently to the flux of incident photons.

We believe that the CA approach may be applied heuristically to a variety phase-change, nonlinear optical and active (nano)phonic systems; for example, the three-level model developed here for Ga may be adapted to VO₂, where ultrafast transitions also appear to involve a transient electronically excited state.^{32–36} In reducing complex systems to a minimally sufficient set of rules and parameters, CA models may not produce the most accurate quantitative fit to the experiment, but their value lies in the provision of simple insight to system dynamics and the relative importance of physical parameters, which can inform the design of further experiments and more refined models. A two-dimensional cellular

array is sufficient here to model the optical properties of an effectively infinite planar metal–dielectric interface illuminated by a plane wave (i.e., as a generic approximation to the experimental realities of Refs. 98 and 99). At the expense of the periodic boundary condition employed in the direction parallel to the interface, the model could readily accommodate inhomogeneous incident beam intensity profiles. Extension to three spatial dimensions would provide for consideration of more complex geometries and finer control of neighbor interaction rules and thresholds (i.e., with 26 surrounding cells in a simple 3D cubic neighborhood as compared to 8 in the 2D square case).

IV. METHODS

A. Cellular geometry

Our CA model employs a two-dimensional square array of cells with a lattice constant $L_c = 0.55$ nm (on the order of the α -gallium crystalline unit cell size¹⁰⁴). The model domain has a depth, in the direction of incident light propagation, of 200 cells (~ 3 times the optical skin depth of α -gallium at the assumed near-infrared illumination wavelength) and a width, parallel to the gallium–silica interface, of again 200 cells (> 20 times the thermal diffusion length in liquid gallium over 1 ps; thermal diffusivity¹⁰⁵ ≈ 0.2 cm²/s). The positional address of each cell is denoted by coordinates i (depth) and j (width), as indicated in Fig. 1(a).

B. Incident photons

We assume incident monochromatic light pulses with either Gaussian or square temporal intensity profiles. In the former case, this gives an absorbed intensity profile of the form

$$I = I_L(1 - R)e^{-4\ln 2(\frac{t}{\tau_p} - 1.5)^2} \quad (1)$$

where I_L is the incident intensity, R is the reflectivity of the Ga–silica interface, and τ_p is the full-width half-maximum pulse duration. Fluence for a Gaussian pulse¹⁰⁶ is given by

$$F_{in} = I_L \tau_p \sqrt{\frac{\pi}{4\ln 2}} \quad (2)$$

and thereby the number of photons entering each CA row j in a given time step is

$$n_0 = \frac{1}{h\tau_p c} \sqrt{\frac{4\ln 2}{\pi}} (1 - R) F_{in} \delta_t L_c^2 \lambda e^{-4\ln 2(\frac{t}{\tau_p} - 1.5)^2} \quad (3)$$

where h is the Planck constant and λ is the vacuum wavelength of incident light.

In the case of a square pulse, $F_{in} = I_L \tau_p$ and the number of photons per CA row per time step is constant during the pulse: $n_0 = \frac{1}{h\tau_p c} (1 - R) F_{in} \delta_t L_c^2 \lambda$.

Under rule 1, a cell in the ground state may absorb one photon with probability $Ab = 0.03$ (a value derived from skin depth; see [supplementary material](#)). A photon not absorbed in cell i passes, within the same time step, sequentially to cells $i + 1$, $i + 2$, etc., until it is absorbed. The probability that a photon will pass through all Ga cells without being absorbed is < 0.0025 .

C. Interface reflectivity

Interface reflectivity R is evaluated in each time step using the transfer matrix method, treating the system as a stack of layers:

- the incident medium is taken to be semi-infinite silica with a relative permittivity $\epsilon_{silica} = 2.28$ (refractive index 1.51);
- at the interface, we assume an ever-present 4-cell ($d_0 = 2.2$ nm) thick surface melt layer of gallium in the metallic state;⁹⁷
- the rest of the $i = 5$ –200 cell thickness of gallium is divided into six layers: five 10-cell layers for pulse durations $\leq 10^7$ fs or 4-cell layers for pulse durations $> 10^7$ fs (for reasons made apparent in Fig. 4) followed respectively by one 146 or 176-cell layer;
- beyond $i = 200$, we assume a semi-infinite thickness of (ground state) α -gallium.

Each CA gallium layer is assigned an effective permittivity calculated as a weighted mean of the α - and liquid gallium permittivities (ϵ_α and ϵ_{liquid} , respectively) according to the number of cells correspondingly in the ground and excited or metallic states: $\epsilon_{eff} = q\epsilon_\alpha + (1 - q)\epsilon_{liquid}$, where q is the filling fraction of ground-state cells.

D. Neighborhood

We utilize a Moore neighborhood,¹⁰² whereby the evolution of each cell in each time step is influenced by the state of the eight surrounding (four nearest and four next-nearest) cells. The model domain is taken to be periodic (or wrapped) in the j direction such that all cells have a full complement of eight neighbors, i.e., rows (i , 1) and (i , 200) are adjacent to one another.

The neighbor number thresholds N_{I2} and N_{2I} , applied under rules 3 and 4, must take values ≥ 5 because lower values are unphysical: in the case of N_{I2} , they can lead to self-sustaining chains of cell conversion adjacent to the persistent surface-melt layer or indeed any column i of all metallic- or excited-state cells. In the case of N_{2I} , they would enable adjacent full columns of metallic-state cells to remain indefinitely in that state.

SUPPLEMENTARY MATERIAL

See the [supplementary material](#) for:

- the dependences of transition probabilities on CA model time step and neighborhood;
- the calculation of photon absorption probability per cell;
- evaluation of the threshold value of Γ_{I2} ;
- the effect of neighbor threshold values N_{I2} , N_{2I} on reflectivity dynamics (in short- and long-pulse regimes);
- representative maps of cellular phase state at the end (as opposed to peak in Fig. 4) of excitation pulses of differing duration, and corresponding dependences of reflectivity on time.

ACKNOWLEDGMENTS

The authors would like to thank E. T. F. Rogers, P. Cencillo-Abad, and V. Savinov for constructive input and discussion.

This work was supported by the UK Engineering and Physical Sciences Research Council (Grant EP/M009122/1), the Singapore Ministry of Education (Grant MOE2016-T3-1-006), and the National Natural Science Foundation of China (Grant U1804165).

DATA AVAILABILITY

Data sharing is not applicable to this article as no new data were created in this study.

REFERENCES

- ¹S. Raoux, *Annu. Rev. Mater. Res.* **39**, 25 (2009).
- ²M. Wuttig and N. Yamada, *Nat. Mater.* **6**, 824 (2007).
- ³J. Lawrence, *Advances in Laser Materials Processing* (Woodhead Publishing, 2018).
- ⁴M. Malinauskas, A. Žukauskas, S. Hasegawa, Y. Hayasaki, V. Mizeikis, R. Buividas, and S. Juodkazis, *Light Sci. Appl.* **5**, e16133 (2016).
- ⁵K. Sugioka and Y. Cheng, *Light Sci. Appl.* **3**, e149 (2014).
- ⁶M. Mao, J. He, X. Li, B. Zhang, Q. Lei, Y. Liu, and D. Li, *Micromachines* **8**, 113 (2017).
- ⁷D. Jin, Q. Chen, T.-Y. Huang, J. Huang, L. Zhang, and H. Duan, *Mater. Today* **32**, 19 (2020).
- ⁸Y. Xie, D. J. Heath, J. A. Grant-Jacob, B. S. Mackay, M. D. T. McDonnell, M. Praeger, R. W. Eason, and B. Mills, *J. Phys.: Photonics* **1**, 035002 (2019).
- ⁹N. I. Zheludev, *Nat. Photon.* **1**, 551 (2007).
- ¹⁰K. J. Miller, R. F. Haglund, and S. M. Weiss, *Opt. Mater. Express* **8**, 2415 (2018).
- ¹¹A. M. Shaltout, V. M. Shalae, and M. L. Brongersma, *Science* **364**, eaat3100 (2019).
- ¹²N. I. Zheludev, *Contemp. Phys.* **43**, 365 (2002).
- ¹³M. Wuttig, H. Bhaskaran, and T. Taubner, *Nat. Photon.* **11**, 465 (2017).
- ¹⁴B. J. Eggleton, B. Luther-Davies, and K. Richardson, *Nat. Photon.* **5**, 141 (2011).
- ¹⁵F. Ding, Y. Yang, and S. I. Bozhevolnyi, *Adv. Opt. Mater.* **7**, 1801709 (2019).
- ¹⁶I. Chakraborty, A. Jaiswal, A. K. Saha, S. K. Gupta, and K. Roy, *Appl. Phys. Rev.* **7**, 021308 (2020).
- ¹⁷T. Alexoudi, G. T. Kanellos, and N. Pleros, *Light Sci. Appl.* **9**, 91 (2020).
- ¹⁸Z. L. Sámson, S.-C. Yen, K. F. MacDonald, K. Knight, S. Li, D. W. Hewak, D. P. Tsai, and N. I. Zheludev, *Phys. Status Solidi - RRL* **4**, 274 (2010).
- ¹⁹B. Gholipour, J. Zhang, K. F. MacDonald, D. W. Hewak, and N. I. Zheludev, *Adv. Mater.* **25**, 3050 (2013).
- ²⁰A. Karvounis, B. Gholipour, K. F. MacDonald, and N. I. Zheludev, *Appl. Phys. Lett.* **109**, 051103 (2016).
- ²¹M. Rudé, R. E. Simpson, R. Quidant, V. Pruneri, and J. Renger, *ACS Photonics* **2**, 669 (2015).
- ²²M. Rudé, J. Pello, R. E. Simpson, J. Osmond, G. Roelkens, J. J. G. M. van der Tol, and V. Pruneri, *Appl. Phys. Lett.* **103**, 141119 (2013).
- ²³A.-K. U. Michel, P. Zalden, D. N. Chigrin, M. Wuttig, A. M. Lindenberg, and T. Taubner, *ACS Photonics* **1**, 833 (2014).
- ²⁴A.-K. U. Michel, A. Hefßler, S. Meyer, J. Pries, Y. Yu, T. Kalix, M. Lewin, J. Hanss, A. De Rose, T. W. W. Maß, M. Wuttig, D. N. Chigrin, and T. Taubner, *Adv. Mater.* **31**, 1901033 (2019).
- ²⁵Q. Wang, J. Maddock, E. T. F. Rogers, T. Roy, C. Craig, K. F. MacDonald, D. W. Hewak, and N. I. Zheludev, *Appl. Phys. Lett.* **104**, 121105 (2014).
- ²⁶Q. Wang, E. T. F. Rogers, B. Gholipour, C. M. Wang, Y. Guanghui, J. Teng, and N. I. Zheludev, *Nat. Photon.* **10**, 60 (2016).
- ²⁷C. Ruiz de Galarreta, A. M. Alexeev, Y.-Y. Au, M. Lopez-Garcia, M. Klemm, M. Cryan, J. Bertolotti, and C. D. Wright, *Adv. Funct. Mater.* **28**, 1704993 (2018).
- ²⁸J. Feldmann, N. Youngblood, C. D. Wright, H. Bhaskaran, and W. H. P. Pernice, *Nature* **569**, 208 (2019).
- ²⁹Y. Ke, S. Wang, G. Liu, M. Li, T. J. White, and Y. Long, *Small* **14**, 1802025 (2018).
- ³⁰M. F. Becker, A. B. Buckman, R. M. Walsler, T. Lépine, P. Georges, and A. Brun, *Appl. Phys. Lett.* **65**, 1507 (1994).
- ³¹A. Cavalleri, C. Tóth, C. W. Siders, J. A. Squier, F. Ráksi, P. Forget, and J. C. Kieffer, *Phys. Rev. Lett.* **87**, 237401 (2001).
- ³²J. Laverock, S. Kittiwatanakul, A. A. Zakharov, Y. R. Niu, B. Chen, S. A. Wolf, J. W. Lu, and K. E. Smith, *Phys. Rev. Lett.* **113**, 216402 (2014).
- ³³V. R. Morrison, R. P. Chatelain, K. L. Tiwari, A. Hendaoui, A. Bruhács, M. Chaker, and B. J. Siwick, *Science* **346**, 445 (2014).
- ³⁴Z. Tao, F. Zhou, T.-R. T. Han, D. Torres, T. Wang, N. Sepulveda, K. Chang, M. Young, R. R. Lunt, and C.-Y. Ruan, *Sci. Rep.* **6**, 38514 (2016).
- ³⁵M. R. Otto, L. P. René de Cotret, D. A. Valverde-Chavez, K. L. Tiwari, N. Émond, M. Chaker, D. G. Cooke, and B. J. Siwick, *Proc. Natl. Acad. Sci. USA* **116**, 450 (2019).
- ³⁶L. Vidas, D. Schick, E. Martínez, D. Perez-Salinas, A. Ramos-Álvarez, S. Cichy, S. Batlle-Porro, A. S. Johnson, K. A. Hallman, R. F. Haglund, Jr., and S. Wall, *Phys. Rev. X* **10**, 031047 (2020).
- ³⁷M. Rini, A. Cavalleri, R. W. Schoenlein, R. López, L. C. Feldman, R. F. Haglund, L. A. Boatner, and T. E. Haynes, *Opt. Lett.* **30**, 558 (2005).
- ³⁸C. Kübler, H. Ehrke, R. Huber, R. Lopez, A. Halabica, R. F. Haglund, Jr., and A. Leitenstorfer, *Phys. Rev. Lett.* **99**, 116401 (2007).
- ³⁹H. W. Liu, L. M. Wong, S. J. Wang, S. H. Tang, and X. H. Zhang, *J. Phys.: Condens. Matter* **24**, 415604 (2012).
- ⁴⁰O. L. Muskens, L. Bergamini, Y. Wang, J. M. Gaskell, N. Zabala, C. H. de Groot, D. W. Sheel, and J. Aizpurua, *Light Sci. Appl.* **5**, e16173 (2016).
- ⁴¹M. J. Dicken, K. Aydin, I. M. Pryce, L. A. Sweatlock, E. M. Boyd, S. Walavalkar, J. Ma, and H. A. Atwater, *Opt. Express* **17**, 18330 (2009).
- ⁴²T. Driscoll, H.-T. Kim, B.-G. Chae, B.-J. Kim, Y.-W. Lee, N. M. Jokerst, S. Palit, D. R. Smith, M. D. Ventura, and D. N. Basov, *Science* **325**, 1518 (2009).
- ⁴³R. M. Briggs, I. M. Pryce, and H. A. Atwater, *Opt. Express* **18**, 11192 (2010).
- ⁴⁴N. A. Butakov, I. Valmianski, T. Lewi, C. Urban, Z. Ren, A. A. Mikhailovsky, S. D. Wilson, I. K. Schuller, and J. A. Schuller, *ACS Photonics* **5**, 371 (2018).
- ⁴⁵J. Rensberg, S. Zhang, Y. Zhou, A. S. McLeod, C. Schwarz, M. Goldflam, M. Liu, J. Kerbusch, R. Nawrodt, S. Ramanathan, D. N. Basov, F. Capasso, C. Ronning, and M. A. Kats, *Nano Lett.* **16**, 1050 (2016).
- ⁴⁶D. Y. Lei, K. Appavoo, F. Ligmajer, Y. Sonnefraud, R. F. Haglund, Jr., and S. A. Maier, *ACS Photonics* **2**, 1306 (2015).
- ⁴⁷C. Wan, E. H. Horak, J. King, J. Salman, Z. Zhang, Y. Zhou, P. Roney, B. Gundlach, S. Ramanathan, R. H. Goldsmith, and M. A. Kats, *ACS Photonics* **5**, 2688 (2018).
- ⁴⁸P. J. Bennett, S. Dhanjal, P. Petropoulos, D. J. Richardson, N. I. Zheludev, and V. I. Emelyanov, *Appl. Phys. Lett.* **73**, 1787 (1998).
- ⁴⁹P. Petropoulos, H. L. Offerhaus, D. J. Richardson, S. Dhanjal, and N. I. Zheludev, *Appl. Phys. Lett.* **74**, 3619 (1999).
- ⁵⁰R. F. Waters, P. A. Hobson, K. F. MacDonald, and N. I. Zheludev, *Appl. Phys. Lett.* **107**, 081102 (2015).
- ⁵¹A. V. Krasavin and N. I. Zheludev, *Appl. Phys. Lett.* **84**, 1416 (2004).
- ⁵²A. V. Krasavin, K. F. MacDonald, N. I. Zheludev, and A. V. Zayats, *Appl. Phys. Lett.* **85**, 3369 (2004).
- ⁵³K. F. MacDonald, A. V. Krasavin, and N. I. Zheludev, *Opt. Commun.* **278**, 207 (2007).
- ⁵⁴S. R. C. Vivekchand, C. J. Engel, S. M. Lubin, M. G. Blaber, W. Zhou, J. Y. Suh, G. C. Schatz, and T. W. Odom, *Nano Lett.* **12**, 4324 (2012).
- ⁵⁵K. F. MacDonald, V. A. Fedotov, and N. I. Zheludev, *Appl. Phys. Lett.* **82**, 1087 (2003).
- ⁵⁶K. F. MacDonald, V. A. Fedotov, S. Pochon, G. Stevens, F. V. Kusmartsev, and N. I. Zheludev, *Eur. Phys. Lett.* **67**, 614 (2004).
- ⁵⁷V. A. Fedotov, K. F. MacDonald, and N. I. Zheludev, *J. Opt. A* **7**, S241 (2005).
- ⁵⁸B. F. Soares, K. F. MacDonald, V. A. Fedotov, and N. I. Zheludev, *Nano Lett.* **5**, 2104 (2005).
- ⁵⁹B. F. Soares, M. V. Bashevov, F. Jonsson, K. F. MacDonald, and N. I. Zheludev, *Opt. Express* **14**, 10652 (2006).
- ⁶⁰B. F. Soares, F. Jonsson, and N. I. Zheludev, *Phys. Rev. Lett.* **98**, 153905 (2007).
- ⁶¹B. F. Soares, K. F. MacDonald, and N. I. Zheludev, *Appl. Phys. Lett.* **91**, 043115 (2007).
- ⁶²S. Pochon, K. F. MacDonald, R. J. Knize, and N. I. Zheludev, *Phys. Rev. Lett.* **92**, 145702 (2004).
- ⁶³A. I. Denisov, K. F. MacDonald, F. J. García de Abajo, and N. I. Zheludev, *Jpn. J. Appl. Phys.* **48**, 03A065 (2009).
- ⁶⁴Y. Gutiérrez, M. Losurdo, P. García-Fernández, M. Sainz de la Maza, F. González, A. S. Brown, H. O. Everitt, J. Junquera, and F. Moreno, *Opt. Mater. Express* **9**, 4050 (2019).
- ⁶⁵Y. Gutiérrez, M. Losurdo, P. García-Fernández, M. Sainz de la Maza, F. González, A. S. Brown, H. O. Everitt, J. Junquera, and F. Moreno, *Adv. Opt. Mater.* **7**, 1900307 (2019).
- ⁶⁶J. Hegedüs and S. Elliott, *Nat. Mater.* **7**, 399 (2008).
- ⁶⁷T. H. Lee and S. R. Elliott, *Phys. Rev. Lett.* **107**, 145702 (2011).

- ⁶⁸S. Senkader and C. D. Wright, *J. Appl. Phys.* **95**, 504 (2004).
- ⁶⁹J. Scoggin, Z. Woods, H. Silva, and A. Gokirmak, *Appl. Phys. Lett.* **114**, 043502 (2019).
- ⁷⁰F. Tabatabaei, G. Boussinot, R. Spatschek, E. A. Brener, and M. Apel, *J. Appl. Phys.* **122**, 045108 (2017).
- ⁷¹S. Meyer, Z. Y. Tan, and D. N. Chigrin, *Nanophotonics* **9**, 675 (2020).
- ⁷²U. Russo, D. Ielmini, A. Redaelli, and A. L. Lacaita, *IEEE Trans. Electron Devices* **53**, 3032 (2006).
- ⁷³X. Ao, H. Xia, J. Liu, and Q. He, *Mater. Des.* **185**, 108230 (2020).
- ⁷⁴Q. Zhang, H. Xue, Q. Tang, S. Pan, M. Rettenmayr, and M. Zhu, *Comp. Mater. Sci.* **146**, 204 (2018).
- ⁷⁵K. Reuther and M. Rettenmayr, *Comp. Mater. Sci.* **95**, 213 (2014).
- ⁷⁶L. Bai, B. Wang, H. Zhong, J. Ni, Q. Zhai, and J. Zhang, *Metals* **6**, 53 (2016).
- ⁷⁷P. Ashwin, B. S. V. Patnaik, and C. D. Wright, *J. Appl. Phys.* **104**, 084901 (2008).
- ⁷⁸C. Mihai and A. Velea, *Model. Simul. Mater. Sci. Eng.* **26**, 045006 (2018).
- ⁷⁹J. L. Guisado, F. Jiménez-Morales, and J. M. Guerra, *Phys. Rev. E* **67**, 066708 (2003).
- ⁸⁰J. G. Kelly and E. C. Boyer, *Cryst. Growth Des.* **14**, 1392 (2014).
- ⁸¹G. H. B. Miranda, J. Machicao, and O. M. Bruno, *Sci. Rep.* **6**, 37329 (2016).
- ⁸²Y. Wang, M. An, Z. Yu, B. Han, and W. Ji, *Constr. Build Mater.* **172**, 760 (2018).
- ⁸³F. Centrone, C. Tassi, M. Barbieri, and A. Serafini, *Phys. Rev. A* **98**, 012105 (2018).
- ⁸⁴A. Bisio, G. M. D'Ariano, and P. Perinotti, *Ann. Phys.* **368**, 177 (2016).
- ⁸⁵V. S. Kalogiton, D. P. Papadopoulos, O. Liolis, V. A. Mardiris, G. C. Sirakoulis, and I. G. Karafyllidis, *IEEE T. Comput. Aid. D.* **36**, 1367 (2017).
- ⁸⁶J. Li and T. C. H. Liew, *Opt. Express* **24**, 24930 (2016).
- ⁸⁷F. Perez-Martinez, K. D. Petersson, I. Farrer, D. Anderson, G. A. C. Jones, D. A. Ritchie, and C. G. Smith, *Microelectr. J.* **39**, 674 (2008).
- ⁸⁸P. Chavel, J. Taboury, F. Devos, and P. Garda, *J. Phys.* **49**, C2-35 (1988).
- ⁸⁹J. F. Botía, A. M. Cárdenas, and C. M. Sierra, *Eng. Appl. Artif. Intel.* **62**, 181 (2017).
- ⁹⁰F. Previdi and M. Milani, *Nuovo Cimento D* **11**, 1625 (1998).
- ⁹¹C. Conti, in *Game of Life Cellular Automata*, edited by A. Adamtzky (Springer, London, 2010).
- ⁹²N. R. Comins, *Phil. Mag.* **25**, 817 (1972).
- ⁹³O. Hunderi and R. Ryberg, *J. Phys. F Met. Phys.* **4**, 2096 (1974).
- ⁹⁴M. Bernasconi, G. L. Chiarotti, and E. Tosatti, *Phys. Rev. B* **52**, 9988 (1995).
- ⁹⁵R. Kofman, P. Cheysson, and J. Richard, *Phys. Rev. B* **16**, 5216 (1977).
- ⁹⁶E. Voloshina, K. Rosciszewski, and B. Paulus, *Phys. Rev. B* **79**, 045113 (2009).
- ⁹⁷R. Trittbach, C. Grutter, and J. H. Bilgram, *Phys. Rev. B* **50**, 2529 (1994).
- ⁹⁸V. Albanis, S. Dhanjal, V. A. Fedotov, K. F. MacDonald, N. I. Zheludev, P. Petropoulos, D. J. Richardson, and V. I. Emel'yanov, *Phys. Rev. B* **63**, 165207 (2001).
- ⁹⁹A. V. Rode, M. Samoc, B. Luther-Davies, E. G. Gamaly, K. F. MacDonald, and N. I. Zheludev, *Opt. Lett.* **26**, 441 (2001).
- ¹⁰⁰O. P. Uteza, E. G. Gamaly, A. V. Rode, M. Samoc, and B. Luther-Davies, *Phys. Rev. B* **70**, 054108 (2004).
- ¹⁰¹B. Chopard and M. Droz, *Cellular Automata Modeling of Physical Systems* (Cambridge University Press, 1998).
- ¹⁰²S. Wolfram, *Cellular Automata and Complexity: Collected Papers* (CRC Press, 1994).
- ¹⁰³V. P. Zhukov and E. V. Chulkov, *Phys-Usp* **52**, 105 (2009).
- ¹⁰⁴V. Heine, *J. Phys. C: Solid State Phys.* **1**, 222 (1968).
- ¹⁰⁵J. T. Schriempf, *Solid State Commun.* **13**, 651 (1973).
- ¹⁰⁶M. E. Povarnitsyn, T. E. Itina, K. V. Khishchenko, and P. R. Levashov, *Appl. Surf. Sci.* **253**, 6343 (2007).